# NUMERICAL MODELLING AND DESIGN OF ALFC SHIELD LOADED BY 20 MM FSP FRAGMENT

Marian Klasztorny, Marek Świerczewski, Paweł Dziewulski, Andrzej Morka

Military University of Technology
Department of Mechanics and Applied Computer Science
Gen. S. Kaliski Street 2, 00-908 Warsaw, Poland
tel.: +48 22 6839947, fax: +48 22 6839355
e-mail: mklasztorny@wat.edu.pl, mswierczewski@wat.edu.pl
pdziewulski@wat.edu.pl amorka@wat.edu.pl

#### Abstract

The study develops numerical modelling and design of the ALFC shield loaded by the 20 mm 54 g FSP fragment moving at impact velocity of 1800 m/s (fragmentation simulation of IED devices), used to protect 5 mm-thick Armox 500T steel plate. The ALFC shield is composed of the ALF energy-absorbing subsystem and a 99.7% Al<sub>2</sub>O<sub>3</sub> alumina ceramic layer. The ALF subsystem is designed to absorb blast wave impact energy induced by explosive materials up to 10 kg TNT. The ceramic layer is aimed at stopping FSP fragments. The 5 mm-thick Armox 500T steel plate reflects the body bottom segment of a light armoured vehicle. The main purpose of the study is to determine the minimum thickness of the ceramic layer at which the 5 mm-thick Armox 500T steel plate is fully protected from perforation. The ALF subsystem has the following layered structure: Al2024 aluminium alloy plate, SCACS hybrid laminate plate, ALPORAS aluminium foam, SCACS hybrid laminate plate. The layers are joined with Soudaseal 2K chemoset glue. SCACS hybrid laminate contains the following components: VE 11-M modified vinylester resin (matrix), SWR800 glass S plain weave fabric, Tenax HTA40 6K carbon plain weave fabric, Kevlar 49 T 968 aramid plain weave fabric. The total thickness of the ALF shield amounts to 76 mm. In the numerical modelling, the aluminium alloy plate and Armox 500T steel plate are working in the elasto-plastic range according to Johnson-Cook model. The 99.7% Al<sub>2</sub>O<sub>3</sub> alumina ceramic is working in elasto-short range according to JH-2 Johnson-Holmquist model. The simulations correspond to large displacements, large deformations and contact among all the components of the system. In FE mesh, the 8-node 24 DOF hexahedral finite elements with single integration point have been used. Additional failure criteria governing ad-hoc erosion of finite elements have been applied. The FEM modelling, simulation and postprocessing have been carried out using Catia, HyperMesh, LS-DYNA and LS-PrePost systems. The simulation results are presented in the form of displacement – perforation contours and the FSP final deformation for both the FSP-shield-plate and the FSP-plate systems. It has been pointed out that 18 mm-thick ceramic layer protects the LAV body bottom plate from perforation.

Keywords: light armoured vehicles, passive protection, IED, FSP, modelling, simulation, design

#### 1. Introduction

Light-armoured vehicles (LAV) are exposed to action of explosive charges in the form of AT mines and IED devices. The latter, apart from blast of explosive material, induce a high-velocity stream of arbitrary shaped fragments, e.g. bearing balls, nails, bolts etc., which are capable of perforation the vehicle floor and wounding/killing the occupants. Modern LAVs commonly have flat-shaped bottoms, which should be equipped with shields against AT-IED charges, having the following features:

- high specific energy of AT/IED blast wave absorption, through various failure mechanisms of the energy-absorbing layers,
- protection of the vehicle bottom from destruction/perforation induced by AT/IED explosion,
- keeping to a minimum plastic deformations of the vehicle body,
- limitation of AT/IED explosion-induced accelerations acting on the occupants to the admissible levels from occupants' health/life point of view.

The literature studies have shown that dissipation of the blast wave energy can be increased reasonably by geometrically advanced energy-absorbing structures, e.g. cylindrical or conical tubes, semi-spherical shells etc., e.g. [10, 11]. However, protective shields with cores composed of such elements are expensive and technologically difficult to manufacturing.

A new anti-AT/IED protective shield applicable to protect LAV vehicles was developed within the framework of research and development project No O R00 0062 06, funded in the period 2009–2010 by National Centre for Research and Development, Poland [7, 8]. The shield, denoted with ALF code, contains layered segments of the following stacking sequence (from the explosion side):

- 1) a 2 mm Al2024 aluminium plate,
- 2) a 9 mm SCACS hybrid laminate,
- 3) a 50 mm ALPORAS aluminium foam core,
- 4) a 9 mm SCACS hybrid laminate.

The layers of ALF segments are integrated with glue joints using Soudaseal 2K chemoset glue; 2 mm-thick glue layers have been performed.

The SCACS hybrid laminates, manufactured using the RTM-vacuum technology, contain the following components:

- a) incombustible VE 11-M vinylester resin,
- b) S-glass plain weave fabric (SWR800, 800 g/m<sup>2</sup>, Hongming Composites CO., Ltd.),
- c) carbon plain weave fabric (Style 430, Tenax HTA40 6K fibres, 300 g/m², 400/400 tex, C. Cramer GmbH & Co. KG Division ECC),
- d) aramid plain weave fabric (Style 328, Kevlar 49 T 968 fibres, 230 g/m², 158/158 tex, C. Cramer GmbH & Co. KG Division ECC).

The glass laminate (S) consists of two layers, carbon laminate (C) -4 layers, and aramid laminate (A) -12 layers. The stacking sequence of the SCACS laminate is  $[0/90]_{12S}$ .

The ALF shields have the following features:

- 1) modularity and integrated plate segments,
- 2) incombustibility, chemical and environment resistance,
- 3) 76 mm thickness,
- 4) 50 kg/m<sup>2</sup> area density,
- 5) high specific-energy absorption,
- 6) replaceability of segments,
- 7) a relatively simple manufacturing, assembly and disassembly technology,
- 8) long durability and relatively low material–manufacturing costs.

The experimental and numerical investigations presented in [7, 8] constitute the basis to assess the ALF shields protection against AT/IED blast wave on level 3b according to standard [13]. On the other hand, the ALF shield does not protect LAVs from IED fragmentation in accordance with requirements set up in [1]. Thus, an additional ultra-hard layer should be applied.

The study develops the ALFC protective system for total anti-AT/IED protection of LAV vehicles. The ALFC shield has layered structure and is composed of the ALF shield and the 99.7% Al<sub>2</sub>O<sub>3</sub> alumina ceramic layer. Two systems are under consideration, denoted with SP and SCP codes. The reference SP system is composed of 76 mm ALF segment and 5 mm Armox 500T plate segment joined with 2 mm Soudaseal 2K glue. The SCP system contains the intermediate layer in the form of 99.7% Al<sub>2</sub>O<sub>3</sub> alumina; three components are joined with 2 mm Soudaseal 2K glue. The main purpose of the study is to determinate the minimum thickness of the alumina ceramic layer in the ALFC system that protects the Armox plate from the 20 mm 54 g FSP perforation. The FSP fragment is moving perpendicularly to the SCP surface at 1800 m/s impact velocity (penetrator). This test simulates fragmentation of IED devices [1, 3].

The problem considered in the study has been solved numerically with the FEM using the following CAE systems: CATIA, HyperMesh, LS-DYNA (a solver), LS-PrePost.

#### 2. Protection of LAV crew-occupants against blast and fragmentation of IED

LAV vehicles operating in any armed conflict zone must satisfy respective requirements in reference to ballistic protection, protection against artillery missile fragmentation, and anti-AT/IED protection. NATO documents [1-3, 13] constitute the basis for making respective requirements in reference to the occupants' protection. However, references [1-3, 13] do not formulate full conditions in reference to IEDs. FSP (Fragment-Simulating Projectile) standard fragments are shown in Fig. 1, [1].

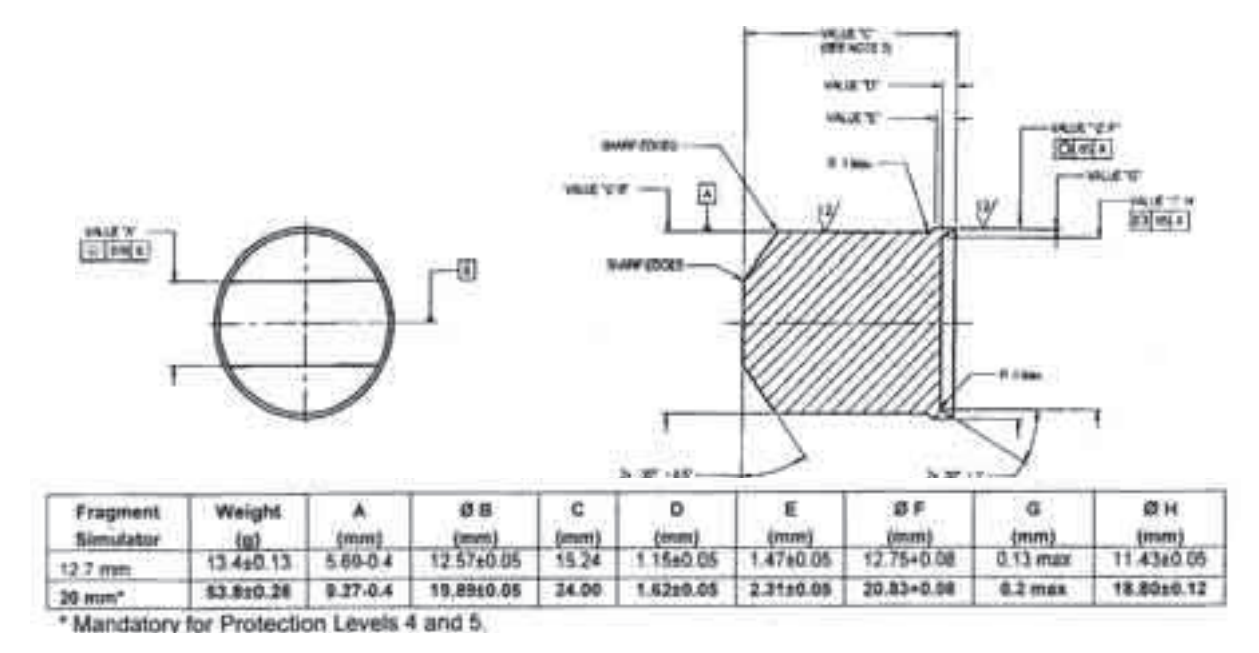


Fig. 1. The FSP standard fragments, [1]

Proposals related to IED fragmentation resistance have been developed in [5, 14]. The IED fragmentation micro-range test has been proposed in [14] with the use of 20 mm 54 g FSP standard fragment compatible with references [1, 13]. The writers [14] assumed the multi-hit mode (6 series with 3 shots each) and the single-hit mode (12 one-by-one shots) for the tested protective shield – protected plate segment. The multi-hit mode is specified in Tab. 1 and illustrated in Fig. 2. Tab. 1 results in the impact kinetic energy  $E_k = 7.3-17.3$  kJ of the damage generator and  $E_k = 52.9-87.5$  kJ of the penetrator.

Size / definition	Value
Maximum distance between shots	75 mm
Shot distance tolerance	0 / +20 mm
Minimum distance to the segment edge	50 mm
Sequence of shots	#1, #2, #3
Impact velocity of shots #1, #2 (damage generators)	$520-800 \text{ m/s} \pm 20 \text{m/s}$
Impact velocity of shot #3 (penetrator)	$1400-1800 \text{ m/s} \pm 20 \text{m/s}$

Tab. 1. The 20 mm 54 g FSP multi-hit mode impacting specification, [14]

In range tests, IED is reflected by one or several 155 mm M107 artillery missiles [14]. Impact angles depend on the vehicle geometry as well as missile location (under the vehicle, on the vehicle side) are commonly equal: 0–360° azimuth, –9° to –40° vertical inclination. Moreover, the writers [14] do not formulate LAV's occupants protection levels in reference to IED blast and fragmentation. Only the maximum level corresponding to 155 mm M107 artillery missile blast and fragmentation under the vehicle has been formulated.

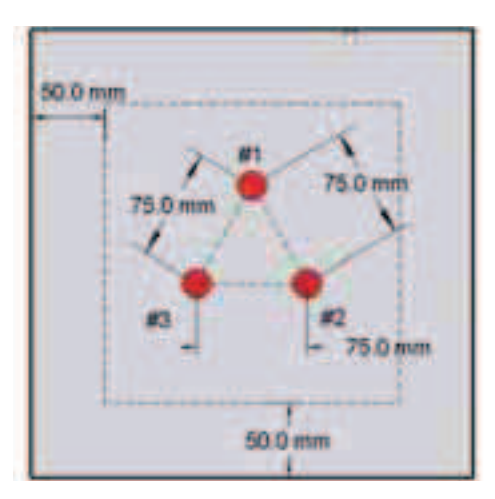


Fig. 2. The multi-hit mode for impacting the protective shield – protected plate segment, [14]

Range tests on 155 mm M107 artillery missile explosion and fragmentation, used to simulate IED, are described in [5]. A 20 mm 54 g FSP fragment with impact velocity >960 m/s is also proposed to simulate IED fragments. The writers have constructed the high dense fragmentation generator in the form of a cylindrical box filled with 2.5 kg TNT and 2 kg of bearing steel bolls (50 g mass and 15 mm diameter each). The impact velocity measured experimentally reached 1750 m/s that corresponds to  $E_k = 76.6$  kJ of each ball. Another FSP fragment proposed in [5] for simulation IED fragmentation had parameters 40 mm 250 g FSP with impact velocity 1500 m/s ( $E_k = 281.2$  kJ).

Advanced and expensive AMAP shields for anti-IED protection of LAVs, tanks, ships and aeroplanes are developed in Ref. [6]. The AMAP system adopts advanced technologies and materials (nano-technologies, composites, ceramics, smart materials, ultra-hard alloys). The AMAP shields also constitute high ballistic protection including PG-7G cumulative missiles.

Numerical modelling of the 0.22 in 17 grains FSP (5.46 mm 1.14 g FSP) impact into  $100 \times 100$  mm two-layer plate (aramid composite, steel) has been developed in [12]. This is the standard fragment in ballistic tests for missile resistant jackets and helmets [15]. The material constants have been taken from [15, 16]. The simulations have been conducted using FE code LS-DYNA. The FSP was modelled as a rigid body, whereas the plate was discretized using 4-node shell elements. The writers considered two impact velocities, i.e. 500 m/s (1800 km/h) and 1000 m/s (3600 km/h); in both cases the protected plated has been perforated.

#### 3. Micro-range tests of the SP system impacted by a 20 mm 54 g FSP

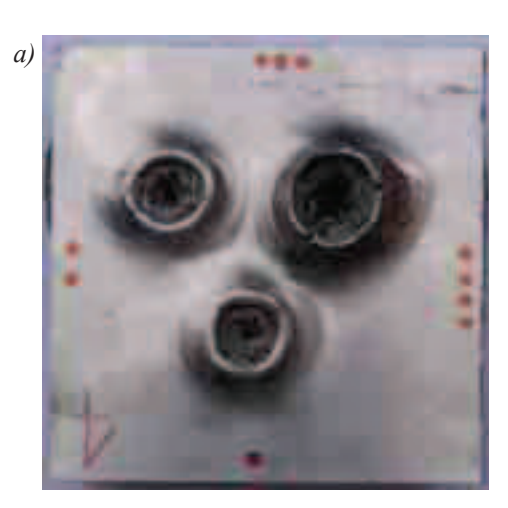
Perforation tests for the SP system impacted by 20 mm 54 g FSP have been conducted in 2010 by Jakusz Co. Ltd., Koscierzyna, Poland. SP square specimens of dimensions 200×200 mm and thickness 76 mm were fixed in the rigid vertical steel frame and hit by FSPs at impact velocities close to values set up in Tab. 1. The impact – penetration – perforation process was registered with Phantom V12 high-speed video camera.

Figure 3 and 4 presents the selected SP specimen after the perforation test according to the multi-hit mode impacting specification given in [9]. Impact velocities amounted to:

- shots #1 and #2: 640 m/s,
- shot #3: 1120 m/s (value lesser by 20% compared to the minimum velocity given in [14]).
   The conclusions resulting from the SP perforation tests are collected below:
- 1) Each shot had induced perforation of the protected plate.
- 2) There had formed shell forgings on the front (Al2024 aluminium) and back (Armox plate) sides of the specimen.
- 3) The ALF layer had eroded cylindrically along with each shot line.

4) Integrity of the SP specimens has been kept. Only light delamination in the glass laminate layers and the glue layer close to the protected plate was observed.

The SP perforation tests confirm necessity of using additional ultra-hard layer; 99.7% Al<sub>2</sub>O<sub>3</sub> alumina has been selected for this purpose.



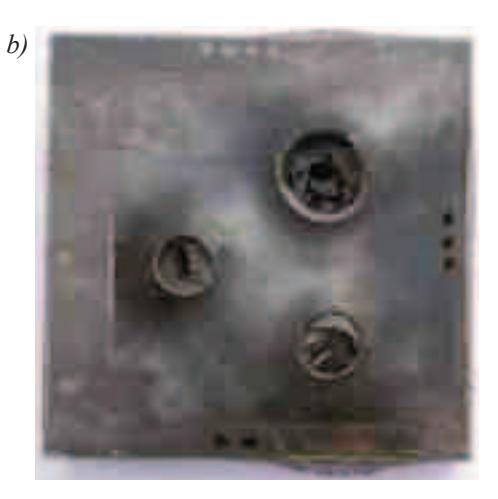


Fig. 3. The selected SP specimen after 20 mm 54 g FSP impacting: a) the front view (Al2024 aluminium), b) the back view (Armox plate)



Fig. 4. The selected SP specimen after 20 mm 54 g FSP impacting – the side view

## 4. Numerical modelling of the SCP system impacted by 20 mm 54 g FSP for specified thicknesses of the ceramic layer

Taking into consideration conclusions resulting from the SP perforation tests (see chapter 3), the overall dimensions of SCP specimens have been decreased to  $100 \times 100 \text{ mm}^2$  in order to simulate a single impact. The specimens were hit centrally and perpendicularly to the front plate by a 20 mm 54 g FSP at 1800 m/s impact velocity. The SCP system has 95–105 mm thickness including a ceramic layer of thickness 10–20 mm. An FSP fragment is made of 4340H cold-rolled annealed alloy steel of  $30\pm2$  HRC hardness or equivalent [1, 14]. The main purpose of the numerical research is to determine the minimum thickness of the ceramic layer that protects Armox 500T steel protected plate against perforation.

The FE model of the FSP–SCP system was developed with CATIA (creating the geometrical models) and Altair HyperMesh (automatic FE meshing) software. LS-PrePost programme was used as a pre-processor for defining all necessary parameters such as boundary conditions, element properties, material properties, the analysis type. The complete FE model was exported as a key file with LS-DYNA preferences. The Lagrangian domain was limited by two planes of symmetry of the system to reduce CPU time. For all simulations, the LS-DYNA nonlinear explicit code was used.

A concept of numerical modelling and simulation of the SCP system impacted by the FSP fragment is described below [4]:

- 1) The external aluminium plate and the protected plate (Armox 500T) are working in the nonlinear elastic-plastic range taking into account high strain rates (Johnson–Cook model). The plates are exposed to large displacements and large plastic deformations.
- 2) The 99.7% Al<sub>2</sub>O<sub>3</sub> ceramic is treated as the nonlinear elastic-short material taking into account high strain rates (JH-2 Johnson–Holmquist model).
- 3) The uniform laminates (S glass, C carbon, A aramid reinforcement), ALPORAS aluminium foam, and Soudaseal 2K glue are described by respective models not taking into account high strain rates. All possible failure mechanisms for these materials as well as large displacements and large deformations are taken into consideration.
- 4) Contact among all components and dry friction between the SCP subsystem and the steel frame are taken into account. The contact was modelled using AUTOMATIC\_SINGLE\_ SURFACE and SEGMENT BASED CONTACT (SOFT 2) options.
- 5) The influence of air and gravitation are neglected.
- 6) Owing to bisymmetry of the system, the FE model has been limited to a quarter of the system. The central zone is meshed with high density whereas the extracentral zone is meshed with medium density (Fig. 5 and 6). In the area contact of the dense and rare meshes, the CONTACT TIED NODES TO SURFACE OFFSET option has been applied.
- 7) The 8-nodes brick finite elements, with 24 DOFs and one integration point, were used taking into account contact and friction phenomena. The FE models are relatively dense and finite elements' dimensions satisfy the aspect ratio requirements before and during the impact/penetration/perforation process. 6 types of hourglass control were included.
- 8) The initial boundary conditions contain the vertical impact velocity of the FSP fragment, fastening of the impacted SCP subsystem in the horizontal rigid steel frame realized as contact of the SCP with the horizontal rigid walls.

Figure 5 presents the simplified numerical model of the 20 mm 54 g FSP standard fragment while the numerical model of the FSP–SCP system is illustrated in Fig. 6.

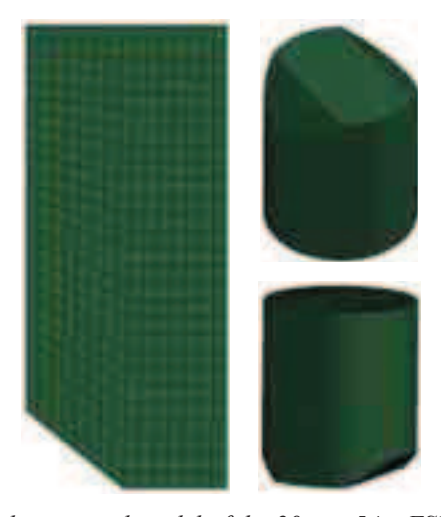


Fig. 5. The simplified numerical model of the 20 mm 54 g FSP standard fragment

Material models for subsequent parts of the FSP-SCP system have been assumed taking into account both Authors' expert knowledge and literature suggestions. In the materials' description original notation of input data assumed in Ref. [15] as well as a system of units used in numerical modelling and simulation (kg, mm, msec, K, GPa, kN) have been saved. The material models used in the modelling are described below:

Armox 500T steel, 4340 steel, and Al2024 aluminium alloy; LS-DYNA material type: MAT\_15 (MAT\_JOHNSON\_COOK) [4]; Equation-of-state: EOS GRUNEISEN; failure model: JC;

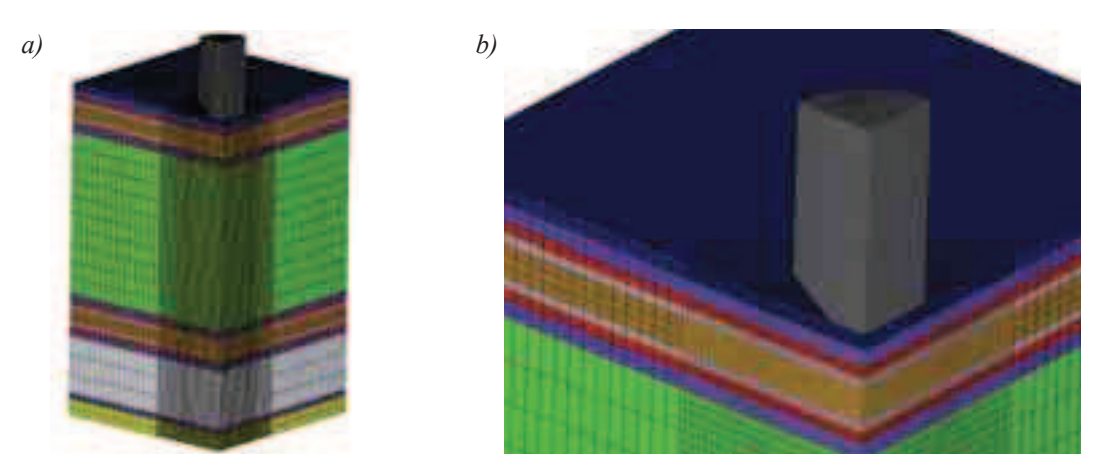


Fig. 6. The numerical model of the FSP-SCP system: a) the axonometric view on the 1/4 part of the system, b) the axonometric view in larger scale

This is the Johnson–Cook strain and temperature sensitive plasticity material, used for problems where strain rates vary over a large range and adiabatic temperature increases due to plastic heating cause material softening. The model requires equation-of-state. The material data are collected in Tab. 2.

Tab. 2. Material data for Armox 500T steel, 4340 steel and Al2024 aluminium alloy, [4, 9]

Parameter	Unit	ARMOX 500T	4340 steel	Al 2024 alloy
Mass density, RO	kg/mm <sup>3</sup>	7.85e-6	7.85E-6	2.81E-6
Shear modulus, G	GPa	79.6	79.6	28.6
Formulation for rate effects: scale yield stress, VP	_	1	0	0
Input constants for the flow stress: A	GPa	0.849	0.792	0.369
В	GPa	1.34	0.510	0.684
N	_	0.0923	0.260	0.730
C	_	0.00541	0.014	0.00830
M	_	0.870	1.03	1.70
Melt temperature, TM	K	1800	1800	775
Room temperature, TR	K	293	293	293
Quasi-static threshold strain rate, EPSO	1/ms	0.001	0.001	0.01
Specific heat, CP	J/(kg·K)	450	450	875
Spall type, SPALL	_	2	2	2
Plastic strain iteration option: accurate iterative solution, IT	_	1	1	1
Failure parameters: D1	_	0	0	-0.969
D2	_	0	0	2.68
D3	_	0	0	4.94
D4	_	0	0	5.145E-4
D5	_	0	0	0.656
Intercept, C	m/s	4570	_	5328
Slope coefficients: S1	_	1.49	_	1.338
S2, S3	_	0	0	0
Gruneisen gamma, GAMAO	_	1.93	_	2.00
First order volume correction, A	_	0.50	_	0.48

Plain woven fabric reinforced uniform laminates;

LS-DYNA material type: MAT\_161 (MAT\_COMPOSITE\_MSC) [4].

This model is addressed to layered composites reinforced with two-directional fabrics. The

model reflects the progressive failure criteria, including delamination. The failure criteria have been established by adopting the methodology developed by Hashin.

The SCACS hybrid laminate, applied in ALF shields developed by the authors [7], is a sequence of uniform laminates S (glass S – vinylester), C (carbon – vinylester), A (aramid – vinylester), modelled as linear elasto-short orthotropic materials after homogenization. The ply sequence in SCACS laminate is  $\{[(0/90)_S]_2, [(0/90)_C]_4, [(0/90)_A]_6\}_s$ . In-plane principal directions  $(0^\circ, 90^\circ)$  are denoted as A and B, whereas out-of-plane principal direction is C. The average values of material constants for S, C, A uniform laminates, based on standard static experiments performed by the authors and partly predicted from the mixtures rule, are collected in Tab. 3.

Tab. 3. The average values of material constants for S, C, A uniform laminates, [4, 7]

Parameter	Unit	S	С	A
Mass density, RO	kg/mm <sup>3</sup>	1.81E-6	1.45E-6	1.24E-6
Young's modulus in longitudinal direction, EA	GPa	29.0	60.0	29.0
Young's modulus in transverse direction, EB	GPa	29.0	60.0	29.0
Young's modulus through thickness direction, EC	GPa	9.8	7.2	3.9
Poisson's ratios: PRBA	_	0.15	0.044	0.080
PRCA = PRCB	_	0.20	0.052	0.070
Shear moduli: GAB	GPa	4.7	4.6	1.4
GBC=GCA	GPa	3.8	3.7	1.1
Material axes option: globally orthotropic, AOPT	_	2	2	2
Layer in-plane rotational angle (degrees), BETA	deg	0	0	0
Longitudinal tensile strength, SAT	GPa	0.439	0.624	0.579
Longitudinal compressive strength, SAC	GPa	0.335	0.580	0.538
Transverse tensile strength, SBT	GPa	0.439	0.624	0.579
Transverse compressive strength, SBC	GPa	0.335	0.580	0.538
Trough thickness tensile strength, SCT	GPa	0.080	0.080	0.080
Crush strength, SFC	GPa	0.393	0.581	0.728
Fibre mode shear strength, SFS	GPa	0.056	0.046	0.031
Matrix mode shear strength in principal planes: SAB	GPa	0.040	0.040	0.040
SBC=SCA	GPa	0.040	0.040	0.040
Scale factor for residual compressive strength, SFFC	_	0.10	0.10	0.10
Material model: fabric layer model, AMODEL		2	2	2
Coulomb friction angle for matrix and delamination failure, PHIC		14	14	14
Element eroding axial strain, E_LIMT	_	5	5	5
Scale factor for delamination criterion, S_DELM		1	1	1
Limit compressive volume strain for element eroding, ECRSH	_	0.89	0.89	0.89
Limit tensile volume strain for element eroding, EEXPN	_	1.11	1.11	1.11

#### ALPORAS aluminium foam;

LS-DYNA material type: MAT 026 (MAT HONEYCOMB) [4].

This material model is useful for honeycomb and foam materials. Nonlinear elasto-plastic behaviour is defined separately for all normal and shear stresses considered fully uncoupled.

After homogenization, ALPORAS foam is modelled as an orthotropic material but its mechanical properties are the same in three orthogonal directions. The elastic moduli vary from the initial non-compacted values to the fully compacted values. The normal stress vs. volumetric strain and the shear stress vs. volumetric strain load curves, in the form corresponding to MAT\_026, are presented in Fig. 7. The proportionality coefficient of these curves equals 0.50 and has been derived from the validation test. Material data, based on the respective static experiments executed by the authors, are given in Tab. 4.

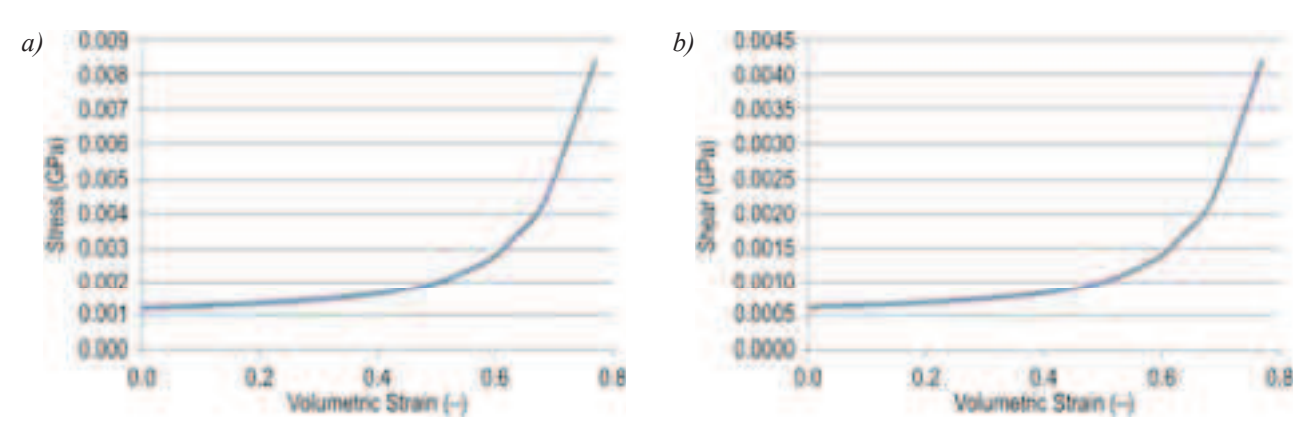


Fig. 7. The normal stress vs. volumetric strain (a) and the shear stress vs. volumetric strain (b) load curves for ALPORAS aluminium foam (extraction of the initial nonlinear elastic response and back extrapolation for small values of the volumetric strain)

Tab. 4. Material constants for ALPORAS aluminium foam described by MAT 026 material model

Parameter		Value
Mass density RO	kg/mm <sup>3</sup>	2.5E-7
Young's modulus for fully compacted material, E	GPa	70
Poisson's ratio for fully compacted material, PR	_	0.33
Yield stress for fully compacted material, SIGY	GPa	0.125
Minimum relative volume for fully compacted material, VF	_	0.23
Material viscosity coefficient, MU	_	0.05
Elastic moduli in uncompressed configuration, EAAU = EBBU = ECCU	GPa	0.193
Shear moduli in uncompressed configuration, GABU = GBCU = GCAU	GPa	0.041

#### SOUDASEAL 2K glue,

#### LS-DYNA material type: MAT 027 (MAT MOONEY-RIVLIN RUBBER) [4].

This is a two-parametric material model for rubber. The axial force vs. actual change in the gauge length,  $\Delta L$ , in the uniaxial tension test is presented in Fig. 8. Material data are based on the experiments performed by the authors: mass density RO = 1.45E–6 kg/mm<sup>3</sup>, Poisson's ratio PR = 0.495, specimen gauge length SGL = 30 mm, specimen width SW = 5.75 mm, specimen thickness ST = 2.3 mm.

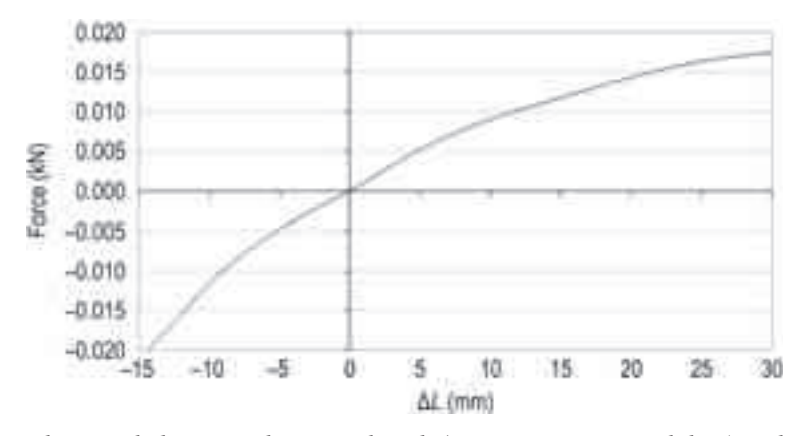


Fig. 8. The axial force vs. the actual change in the gauge length (average experimental data) in the uniaxial tension test for SOUDASEAL glue

### 99.7% $Al_2O_3$ corundum ceramics;

LS-DYNA material type: MAT\_110 (MAT\_JOHNSON\_HOLMQUIST\_CERAMICS) [4]; Equation-of-state: in the polynomial form without the thermal component; failure model: JH-2.

This Johnson–Holmquist Plasticity Damage Model is useful for modelling ceramics, glass and other brittle materials. The material constants of 99.7% Al<sub>2</sub>O<sub>3</sub> corundum ceramics are taken from [9] and cited in Tab. 5.

Parameter	Unit	Value
Density, RO	kg/mm <sup>3</sup>	3.89E-6
Shear modulus, G	GPa	152.0
Material constants for JH-2 model:		
<ul> <li>Intact normalized strength parameter, A</li> </ul>	_	0.88
<ul> <li>Fractured normalized strength parameter, B</li> </ul>	_	0.45
<ul> <li>Strength parameter (for strain rate dependence), C</li> </ul>	_	0.007
<ul> <li>Fractured strength parameter (pressure exponent), M</li> </ul>	_	0.6
<ul> <li>Intact strength parameter (pressure exponent), N</li> </ul>	_	0.64
Maximum tensile pressure strength, T	GPa	0.462
Hugoniot elastic limit, HEL	GPa	7.0
Fraction of elastic energy loss converted to hydrostatic energy	_	1
(affects bulking pressure that accompanies damage), BETA		
Maximum normalized fractured strength, SFMAX	_	1
Reference strain rate, EPSI	1/ms	0.001
Coefficients in the equation-of-state: K1	GPa	231
K2	GPa	-160
K3	GPa	2774
Parameters in the failure model: D1	_	0.0125
D2	_	0.7
FS	_	0.0

Tab. 5. Material constants for 99.7% Al<sub>2</sub>O<sub>3</sub> corundum ceramics, [4, 9]

Additional erosion criteria has been set up with MAT\_ADD\_EROSION card taking into consideration the ultimate strains at failure, i.e. effective strains EFFEPS, bulk strains VOLEPS, and shear strains ESPPH. Assumed values, based on [16], are collected in Tab. 6 where DMGEXP is the exponent for nonlinear damage accumulation.

Component	EFFEPS	VOLEPS	EPSSH	DMGEXP
ALPORAS	0	0.05	0.5	1
S laminate	0	0.05	1	1
C laminate	0	0.05	1	1
A laminate	0	0.05	1	1
ARMOX 500 T	0	0.05	1	1
Al 2024	0	0.05	1	1
Soudaseal 2K	0.5	0.1	0.5	1
4340 steel	0	0.05	1	1
99.7% Al <sub>2</sub> O <sub>3</sub> ceramics	0	0.05	1	1

Tab. 6. Parameters of the additional erosion criteria [4, 9]

#### 5. The simulation results

The computations have been conducted at Department of Mechanics and Applied Computer Science, Military University of Technology, Warsaw, Poland using FE code LS-Dyna v971. Four series have been performed, respectively for thickness 10, 18, 19, and 20 mm of the ceramic layer.

Figures 9–12 present the total displacement contours in the FSP–SCP system in order to illustrate the impact/penetration/perforation process. The contours show that FSP fragment creates

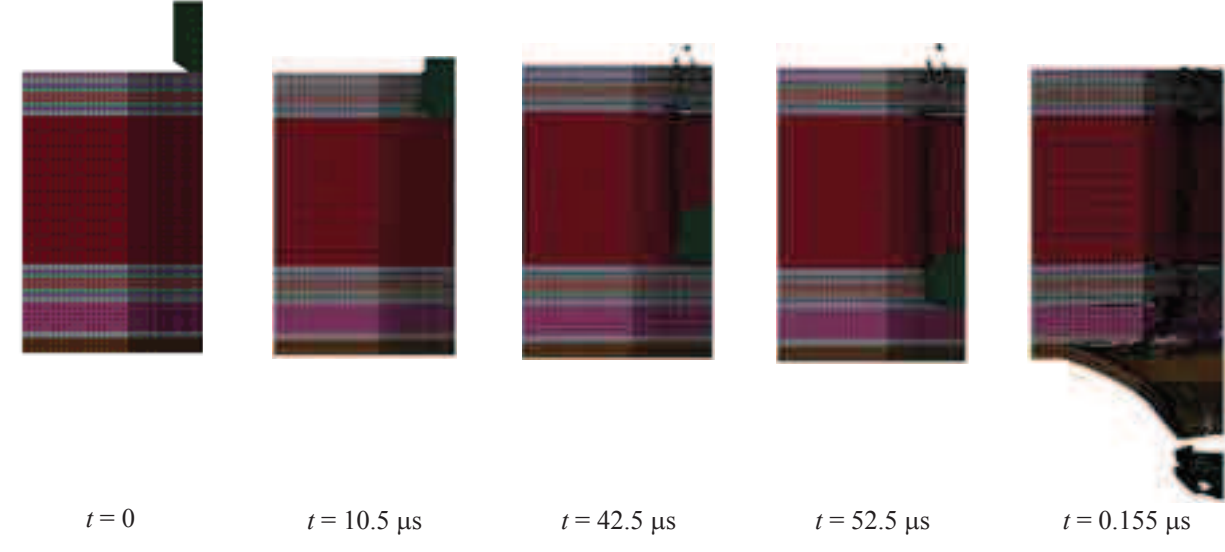


Fig. 9. Displacement contours of the FSP-SCP system at selected time points, for 10 mm thick ceramic layer

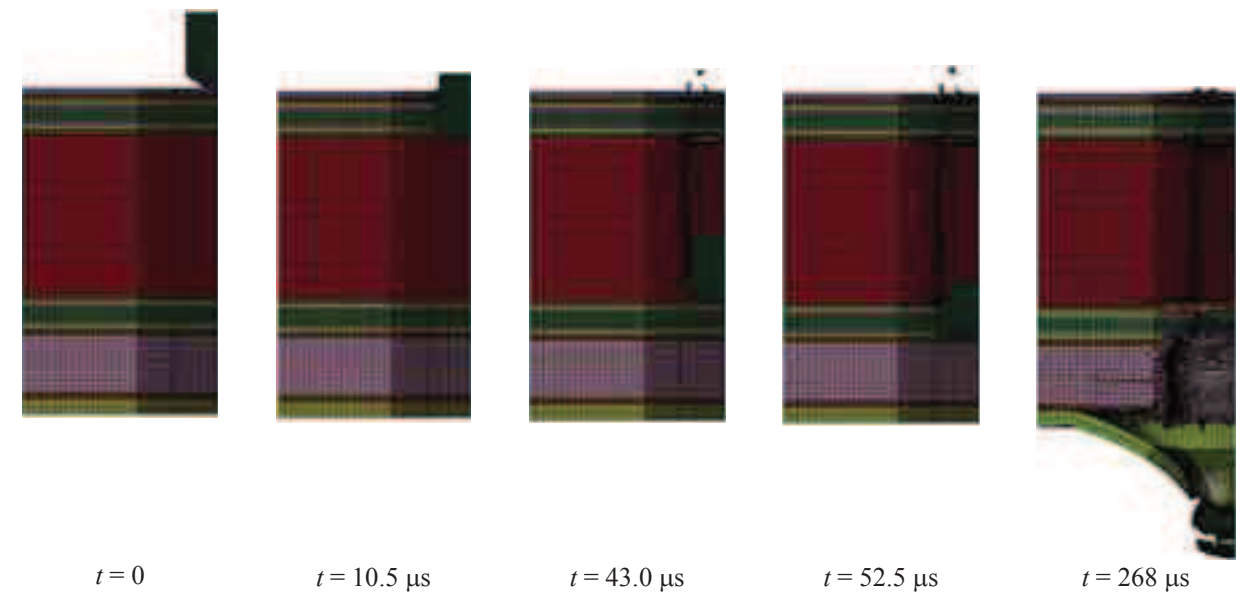


Fig. 10. Displacement contours of the FSP-SCP system at selected time points, for 18 mm thick ceramic layer

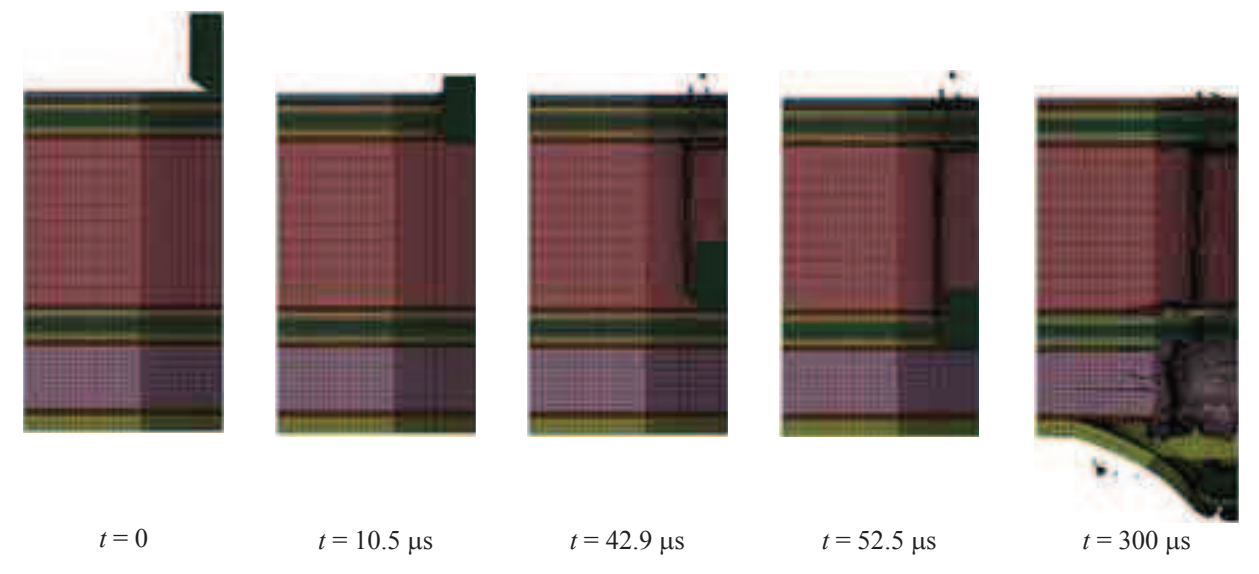


Fig. 11. Displacement contours of the FSP-SCP system at selected time points, for 19 mm thick ceramic layer

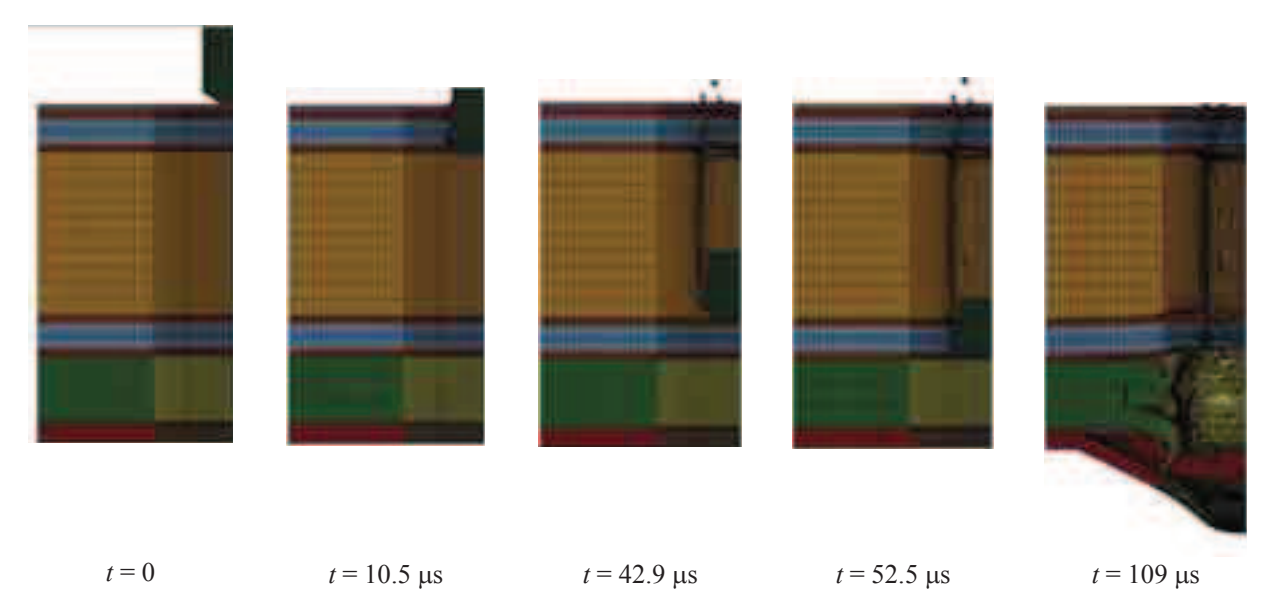


Fig 12. Displacement contours of the FSP-SCP system at selected time points, for 20 mm thick ceramic layer

a quasi-cylindrical crater and deforms plastically progressively during the penetration via the ALFC shield. Perforation of the 5 mm ARMOX 500T protected plate occurs at ceramics thickness 10–18 mm. For 19 mm thickness, the FSP fragment induces cracking of the protected plate, whereas for 20 mm thickness, the fragment is fully stopped but plastic deformations of the protected plate are large.

Diagrams of the kinetic energy of 20 mm 54 g FSP fragment during the impact/ penetration/ perforation process are depicted in Fig. 13 for analysed thicknesses of the corundum ceramic layer. There is only reflected the end phase corresponding to [0.05 ms, 0.20 ms] time interval. The diagrams illustrate the energy loss during penetration of subsequent components and confirm the conclusion of full protection of the vehicle bottom for 20 mm thick ceramic layer.

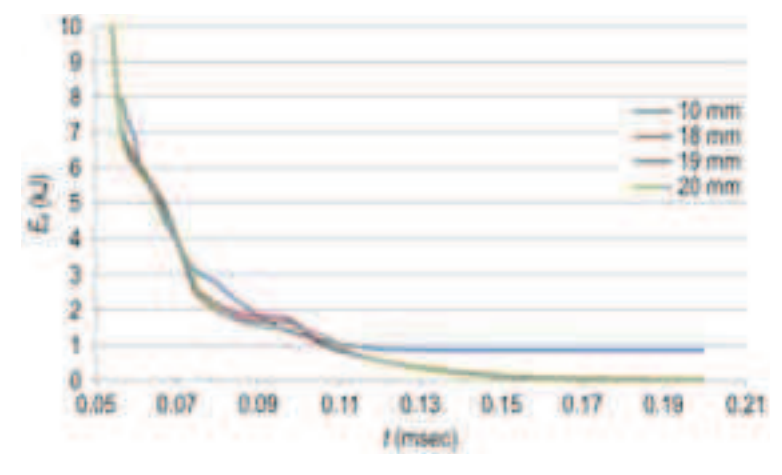


Fig. 13. Diagrams of the 20 mm 54 g FSP kinetic energy in [0.05 ms, 0.2 ms] time interval, for selected ceramic layer thicknesses

#### 6. Final conclusions

The study develops the original ALFC shield for protection of light armoured vehicles against AT mines and IED devices blasts. The vehicle body bottom is in the form of a 5 mm ARMOX 500T steel plate. The ALFC shield has sophisticated structure, in which numerous material properties as well as failure mechanisms have been utilized in order to achieve the high level of the vehicle protection.

The numerical model of the FSP–SCP system has been validated positively using 12.7 mm 13.4 g FSP fragment (the publication in progress).

Application of the ALF shield and 20 mm thick 99.7% Al<sub>2</sub>O<sub>3</sub> corundum ceramic layer ensures protection of a 5 mm Armox 500T steel plate against perforation of the 20 mm 54 g FSP fragment at 1800 m/s impact velocity.

#### References

- [1] AEP-55, Volume 1 (Ed. 1), Procedures for Evaluating the Protection Levels of Logistic and Light Armoured Vehicles for KE and Artillery Threats, NATO/PFP Unclassified.
- [2] AEP-55, Volume 2 (Ed. 1), Procedures for Evaluating the Protection Levels of Logistic and Light Armoured Vehicle Occupants for Grenade and Blast Mine Threats Level, NATO/PFP Unclassified.
- [3] DGLEPM DGLEPM T & E Engineering Std, Improvised Explosive Device Protection Systems, LOI/P&A for TAPV Project, Unclassified.
- [4] Hallquist, J. O. (Ed.), LS-DYNA V971 R4 Beta. Keyword User's Manual, LSTC Co., CA, USA 2009.
- [5] http://www.ibd-deisenroth-engineering.de/amap-ied.html.
- [6] Karpenko, A., Ceh, M., Experimental Simulation of Fragmentation Effects of an Improvised Explosive Device, 23rd International Symposium on Ballistics, Tarragona, Spain 2007.
- [7] Klasztorny, M., Dziewulski, P., Niezgoda, T., Morka, A., *Modelling and Numerical Simulation of the Protective Shield Protected Plate Test Stand System Under Blast Shock Wave*, Journal of KONES Powertrain and Transport, Vol. 17, No. 3, pp. 197-204, 2010.
- [8] Klasztorny, M., Niezgoda, T., Panowicz, R., Gotowicki, P., *Experimental Investigations of the Protective Shield Protected Plate Test Stand System Under Blast Shock Wave*, Journal of KONES Powertrain and Transport, Vol. 17, No. 4, pp. 229-236, 2010.
- [9] Morka, A., *Material Data Basis*, Research Report (unpublished), Military University of Technology, Warsaw, Poland 2010.
- [10] Niezgoda, T., Ochelski, S., Barnat, W., *Analysis of Impact Energy Absorption by Selected Composite Structures* [in Polish]. Mechanical Review [Przegląd Mechaniczny], No. 9, 2006.
- [11] Niezgoda, T., Barnat, W., *Numerical-Experimental Investigation of Failure Energy of Composite Energy Absorbing Panels*, Journal of KONES Powertrain and Transport, Vol. 14, No. 4, pp. 307-318, 2007.
- [12] Niezgoda, T., Kosiuczenko, K., Barnat, W., Panowicz, R., *Numerical Analysis of Impact of the Fragment into the Layered Plate* [in Polish], Open-Cast Mining [Górnictwo Odkrywkowe], Vol. 59, No. 3, pp. 61-64, 2010.
- [13] STANAG 4569 (Ed. 1), Protection Levels for Occupants of Logistic and Light Armoured Vehicles, NATO/PFP Unclassified.
- [14] STANAG 4190, Test Procedures for Measuring Behind-Armour Effects of Anti-Armour Ammunition, NATO/PFP Unclassified.
- [15] MIL-DTL-46593B (MR), Detail Specification. Projectile, calibres .22, .30, .50 and 20 mm fragment-simulating, Department of Defense, USA 2008.
- [16] Tham, C. Y., Tan, V. B. C., Lee, H. P., *Ballistic Impact of a Kevlar Helmet. Experiment and Simulations*, International Journal of Impact Engineering, Vol. 35, No. 5, pp. 304-318, 2008.